

The influence of thickness on the mechanical behavior of carbon/epoxy laminates

Pedro Eliezer de Araújo Júnior, mscpedro@ita.br

Sergio Frascino Müller de Almeida, frascino@ita.br

Department of Mechanical Engineering, Instituto Tecnológico de Aeronautica, Praça Marechal Eduardo Gomes 50, CEP 12228-900 Sao Jose dos Campos, SP, Brazil

Antonio Claret, claret@dem.inpe.br

Control and Space Mechanics Division, Instituto de Pesquisas Espaciais, Av. dos Astronautas 1758, CEP 12227-010 Sao Jose dos Campos, SP, Brazil

Abstract. *Thermal residual stresses arise during manufacture of polymer composite laminates and may affect the elastic and strength properties. In this work, the residual stresses are characterized by the curvature of non-symmetric laminates. A [0/90] carbon/epoxy plate was cut into six strips, three along the direction of the reference axis (0°) and three rotated along the 90° direction. After cure, due to the fact that this laminate is non-symmetric, the strips presented curvature at room temperature. All strips were subjected to a mechanical loading, and their changes of curvature were measured using image analysis techniques. Measurements were performed for twelve different loads, ranging from 0 to 0.3 N. A numerical model in Abaqus was developed to simulate the elastic behavior for each of the twelve experimental points. The thicknesses of the laminate were measured and the thickness of each layer was measured by micrography. The plots showed a good correlation between the curves generated by Abaqus and measured results. The layer thicknesses clearly influences the results.*

Keywords: *composites, curvature, micrograph, finite elements*

1. INTRODUCTION

In recent years the researches on composite materials have been intensified as their use is being expanded in aeronautical and aerospace industries. In particular, laminated polymeric composites are characterized by design flexibility, anisotropy, simple processing, low density, chemical resistance, high damping, thermal stability, thermal insulation, thermal conductivity, wear resistance, long life fatigue, acoustic insulation, corrosion resistance, high strength, high stiffness. As a consequence, composites primary structures can be produced with weight and cost savings (Daniel and Ishai, 2006).

Composite materials have become increasingly popular due to their considerable stiffness and strength to weight ratio. In particular, aerospace structures use more composite materials to reduce the structural weight. Anisotropy is the main characteristic of composite materials and is an advantage from the perspective of structural design. However, it is also an important cause of complicated failure mechanisms (Oh *et al*, 2006). A large amount of research has been dedicated to solve the issues involved in composite structural design; this work is a contribution towards this goal.

Thermal cycles results in variations in thermal and mechanical properties of the material. Therefore, complex residual stresses appear. The change in composites microstructure after forming is influenced by various possible mechanisms such as thickness variation, fiber orientation, fiber slippage, and fiber volume fraction throughout the molded part the change in microstructure (Baillargeon and Vu-khanh, 2001).

Recently, Parlevliet *et al.* (2007) report that experimental studies have shown that residual stresses in composites may decrease significantly during storage under ambient hygrothermal conditions (room temperature ~23°C and ~50% relative humidity). The curvature of nonsymmetrical laminates under room temperature decrease with time due relaxation of residual stresses. Temperature, time, humidity, viscoelastic oxygen-rich environment may alter the value of the glass transition temperature (T_g) or the stress-free temperature resulting in decrease of some composite properties.

The combination of vacuum and different coefficients of thermal expansion between the laminate and mold of cure results in the lack of homogeneity of the material along the thickness of the laminate. The anisotropy of the coefficients of thermal expansion produces surface tension on the resin surface in contact with the mold. The vacuum on the surface opposite to the mold promotes migration of resin across the laminate thickness. As a result, the cured laminate is resin rich in the side of the mold and resin starved in the side of the vacuum application (Radford, 1993; Radford and Fu, 2003).

2. EXPERIMENTAL PROCEDURE

2.1 Sample description and micrographs

All samples were extracted from the [0/90] carbon/epoxy plate, while five were cut along the direction of the reference axis (0°) and five rotated along the 90° direction. They were cold mounting, grinding, polished and photographed. Cold mounting is especially suited for mounting specimens that are sensitive to heat or pressure. Grinding is the first stage in mechanical material removal. Proper grinding removes damaged or deformed surface material while introducing as little new deformation as possible, thus preparing the sample surface for polishing. Grinding is divided into two processes: plane grinding and fine grinding. This stage were used sandpapers of 100, 220, 600, 1500, then diamond paste of $9\mu\text{m}$ and colloidal silica.

Five images were recorded for each sample along its length. The images were obtained using a Carl Zeiss microscope, Sony digital camera and image-capture program, Image Pro-Express 4.5.1.3. The samples are shown in Fig. 1.

Figure 2 is the image obtained from sample 3-1, which shows that the layer of the right is much thicker than the layer on the left. One can note the variation in thickness along the length.



Figure 1. Embedded samples

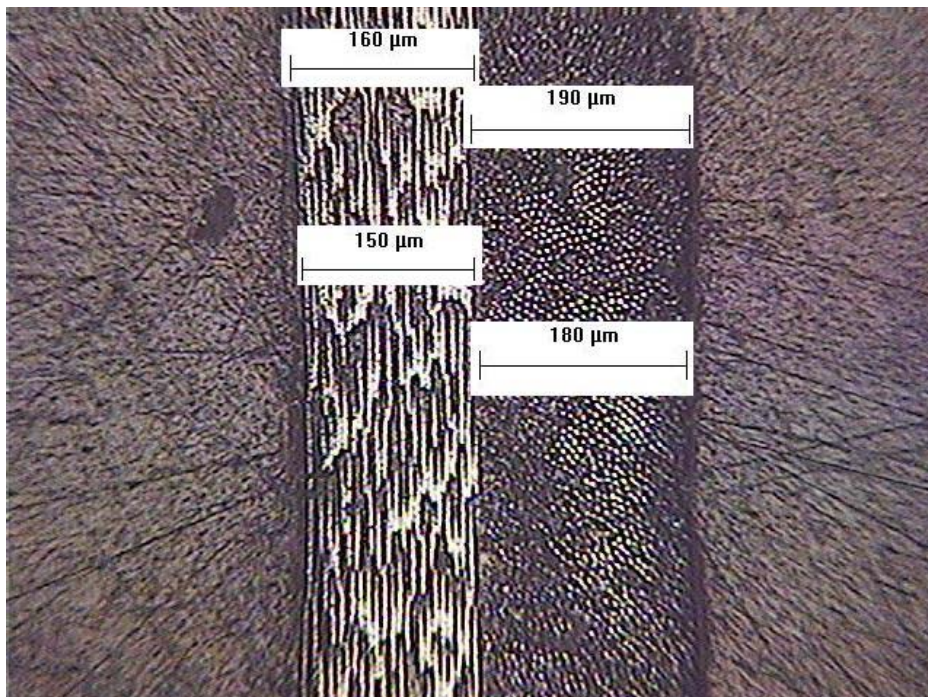


Figure 2 – Difference between the thicknesses of the layer

A subroutine in Matlab was developed to read all the pixels per line at segments defined by three selected points. The first point was chosen at the top layer of the left; the second point was located at the end of the first layer and the beginning of the second layer. Finally, the third point was located at the end of the second layer. The distance between the points is the thickness of the layer for each line. Finally, the average thickness of each layer and its standard deviation were computed. Table 1 shows the average and standard deviation per sample for each layer.

Table 1 – Results of micrographs of 10 samples

Sample	Layer 0° (µm)	Layer 90° (µm)
1	161.3 ± 9.5	175.4 ± 6.8
2	181.7 ± 3.3	178.3 ± 6.6
3	155.1 ± 4.4	175.2 ± 5.4
4	187.2 ± 3.6	181.3 ± 4.9
5	182.4 ± 9.5	188.2 ± 10.3
6	183.6 ± 13.4	181.9 ± 12.0
7	183.5 ± 8.7	185.6 ± 9.2
8	181.7 ± 7.6	183.2 ± 8.1
9	191.6 ± 16.9	180.1 ± 9.8
10	196.2 ± 15.6	182.6 ± 11.3
average	180.4 ± 9.2	181.2 ± 8.4

2.2 Specimens and layers thicknesses

Nine strips were cut from the plate. Three strips were taken from the center at an angle of 45°. Three strips were extracted along the direction of the reference axis (0°). The strip received the nomenclature from the left to right: (3A_0_1S), (3A_0_2S and 3A_0_3S). Three strips were cut at 90°: (3A_90_1S) (3A_90_2S) and (3A_90_3S) from left to the right.

All strips were measured in three points along three dimensions (length, width and thickness). Measurements were performed using a measuring coordinate machines by Mitutoyo and also with a micrometer with accuracy of ± 2.5µm, (ASTM, 2005). The average length was ±1mm, the average width of 12 ± 0,2mm. All strips had different curvatures as it can be seen in the Fig. 3.

The thicknesses were measured at 54 points along the length. A variation in thickness along the length can be observed in Tab. 2. Some researchers observed that the variation in thickness occurs during the manufacturing process of composites (Baillargeon and Vu-khanh, 2001; Laroche and Vu-Khanh, 1994).

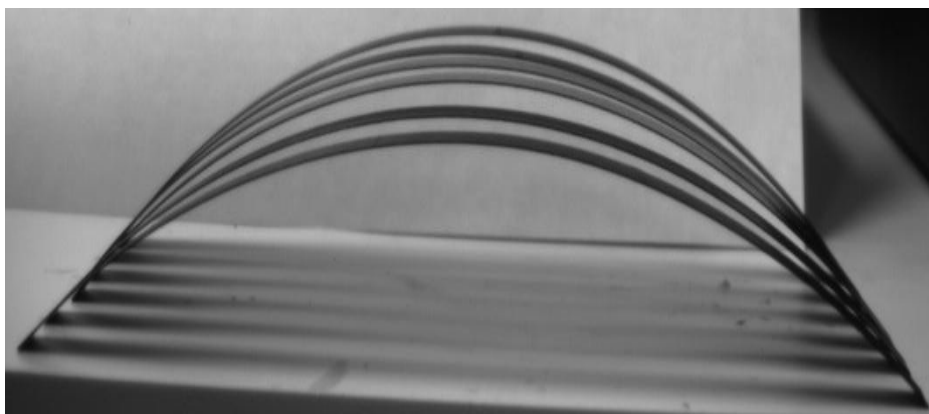


Figure 3. Curvatures of the strips

Table - 2: Laminate thickness along the length

Laminate thickness(mm)	3A_0_1S	3A_0_2S	3A_0_3S	3A_90_1S	3A_90_2S	3A_90_3S
1	0.379	0.391	0.395	0.382	0.398	0.391
2	0.392	0.397	0.400	0.391	0.408	0.396
3	0.401	0.400	0.400	0.393	0.406	0.397
4	0.4	0.401	0.398	0.379	0.397	0.395
5	0.383	0.395	0.394	0.386	0.394	0.399
6	0.394	0.397	0.395	0.385	0.398	0.398
7	0.396	0.401	0.387	0.384	0.395	0.396
8	0.409	0.403	0.388	0.385	0.399	0.392
9	0.406	0.400	0.390	0.387	0.397	0.391
10	0.392	0.397	0.389	0.381	0.401	0.385
11	0.401	0.404	0.388	0.381	0.399	0.37
12	0.383	0.409	0.389	0.386	0.401	0.368
13	0.379	0.407	0.39	0.388	0.405	0.377
14	0.387	0.405	0.393	0.375	0.402	0.377
15	0.388	0.404	0.392	0.383	0.400	0.368
16	0.39	0.399	0.392	0.38	0.403	0.37
17	0.389	0.400	0.403	0.377	0.392	0.393
18	0.382	0.400	0.404	0.373	0.382	0.393
19	0.39	0.399	0.405	0.375	0.388	0.393
20	0.392	0.393	0.4	0.366	0.375	0.372
21	0.389	0.401	0.396	0.374	0.382	0.373
22	0.391	0.397	0.397	0.376	0.375	0.382
23	0.397	0.403	0.394	0.374	0.392	0.371
24	0.401	0.391	0.392	0.376	0.379	0.382
25	0.395	0.402	0.388	0.371	0.38	0.383
26	0.392	0.402	0.393	0.377	0.373	0.395
27	0.393	0.394	0.392	0.369	0.377	0.408
28	0.393	0.395	0.400	0.371	0.381	0.415
29	0.389	0.404	0.399	0.378	0.391	0.417
30	0.396	0.406	0.401	0.367	0.408	0.418
31	0.408	0.415	0.408	0.373	0.413	0.419
32	0.407	0.416	0.404	0.374	0.418	0.42
33	0.4	0.412	0.408	0.377	0.414	0.413
34	0.4	0.406	0.41	0.371	0.415	0.419
35	0.407	0.404	0.412	0.379	0.414	0.415
36	0.402	0.404	0.403	0.374	0.417	0.414
37	0.404	0.409	0.41	0.393	0.414	0.405
38	0.4	0.411	0.421	0.39	0.41	0.398
39	0.398	0.414	0.411	0.394	0.421	0.408
40	0.397	0.413	0.412	0.39	0.421	0.415
41	0.392	0.415	0.411	0.396	0.414	0.417

Laminate thickness(mm)	3A_0_1S	3A_0_2S	3A_0_3S	3A_90_1S	3A_90_2S	3A_90_3S
42	0.394	0.414	0.406	0.394	0.408	0.421
43	0.400	0.411	0.407	0.399	0.416	0.422
44	0.404	0.408	0.412	0.398	0.420	0.428
45	0.404	0.409	0.401	0.393	0.423	0.424
46	0.403	0.41	0.399	0.392	0.43	0.424
47	0.411	0.414	0.396	0.397	0.44	0.424
48	0.408	0.412	0.398	0.400	0.426	0.42
49	0.407	0.416	0.397	0.396	0.423	0.409
50	0.405	0.418	0.413	0.400	0.420	0.406
51	0.407	0.421	0.404	0.404	0.420	0.404
52	0.402	0.424	0.412	0.407	0.422	0.407
53	0.414	0.426	0.407	0.408	0.42	0.405
54	0.415	0.416	0.407	0.401	0.414	0.402
layer thickness average	0.199	0.203	0.200	0.192	0.202	0.200
standard deviation	0.0086	0.0082	0.0082	0.01086	0.01588	0.01730

2.3 Experimental set-up

Palerosi and Almeida (2007) developed a device to assist in the image measurement. A flat base plate was used to support the specimens during the tests. Two reference marks were traced in the base plate in such a way that they were always captured together in the images. Since the distance between the reference marks is known, it was possible to calibrate the measured values in pixels. Attached to the base plate, in the background of the specimen, a white painted plate provided a contrast to the acquired images. In order to avoid any undesirable motion of the sample, one of the sample edges was taped to the base plate. The opposite edge was allowed to slide over a smooth surface coated with a Kapton® tape; this decreased the friction between the sample and the base plate. Thus, it is assumed that the influence of the test device on the results is minimal. A line is attached the specimens via a pulley is then attached to a container, thereby simulating a tensile test. The masses are introduced in the container, thereby increasing traction on the free specimen, thereby varying the curvature, as can be seen in Fig. 4. All masses used in the experiment were weighed in analytical balance Mettler AL204 resolution of 0.1 mg and standard deviation of 0.1 mg. Value was adopted as the mass unit is the average of 50 heavy weights, $m = 0.5747g$.



Figure 4. Specimen and test device

2.4 Load-curvature- experiments

The load-curvature experiments were performed from zero to thirty masses in three masses steps resulting in a total of twelve points. An image was acquired at each load. All images were acquired at a temperature of 20°C. The images were processed using specifically developed mathematical routines running in MATLAB®. Microsoft Paint® was used to select the region of interest in the original images before processing with the MATLAB® routines.

In MATLAB®, initially an approximation of the image is used as reference to delete spurious points. The least-squares method is applied to interpolate the remaining points and fit the best arc to compute the radius of curvature. At this point, the circumference radius, and consequently the curvature, is defined in pixels and a dimensionalization is needed. An additional routine captures the reference marks traced on the test device base plate and calculates the multiplication factor to be applied to yield measurements in mm.

A plot of the final curvature and of the valid and suppressed points was implemented to allow a visualization of the curve fitting process. The routine also provides the standard deviation of the readings based on the approximation method applied. The maximum standard deviation was to be found about 0.03% of the experimental curvature. The small magnitude indicates that the shape of the curved specimens is a nearly a perfect arc of circumference no other numerical evaluation was performed to verify the sample shape. The curvature is found from the relation $\kappa=1/R$, where R is the radius of curvature at the laminate.

2.5 Digital imaging process calibration

With the purpose of calibrating the measuring system by image, a pattern was machined from an aluminum plate with dimensions (300x230x12) mm. Holes were machined in this plate. The holes were aligned with respect to the baseline of the piece, serving as a reference for the images. Distance between points was measured to establish a relationship of scale between mm and the measurement system of the image, pixels. The curves were generated is based on the radii 90, 200, 300, 400, 700, 1000 and 1300 mm.

The measurement system uses as a reference image by the white and black pixels. After machining the plate was anodized in black by forming an aluminum oxide layer by an electrolytic process. Then the plate was painted with synthetic enamel white matte, typical for metals as shown in Fig. 5. The linear distance between points on the plate and all curves were measured using a machine for measuring coordinates (MMC), model Crysta-Apex C7106, Mitutoyo.

The points obtained by the machine are used to estimate the radius of the curves. The coordinates can be read by scanning or point-to-point. A reading of sections was performed by scanning. Scanning was defined by a starting point, an end point, the geometric element and the step. The element chosen was the geometric circle. For each curve two scans were performed, one internal and one external. The program interpolates the two diameters generating a new diameter that best fits the images. Images of the plate were acquired and measured through the program and found errors below 1%.

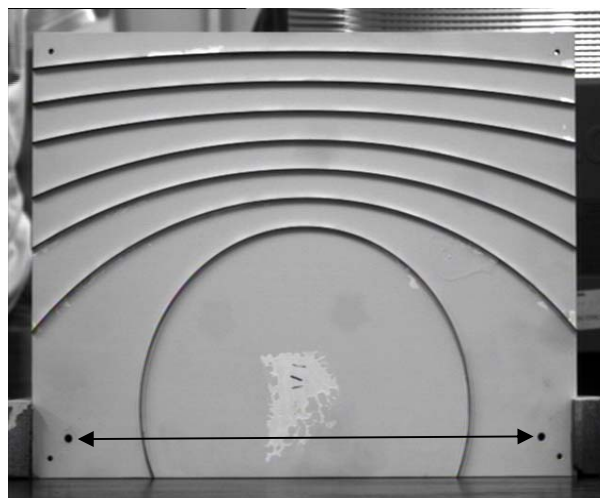


Figure 5. Calibration plate

2.6 Finite elements analyses

The finite element model presented in this study has been developed using ABAQUS® 6.5-1 software. Six different models were developed, one for each strip. Each model was built based on the value of the flexural curvature measured by the method of measurement by image processing without external loading and constant room temperature of 20°C. All models were developed from an initial curvature, according can to Fig. 6.

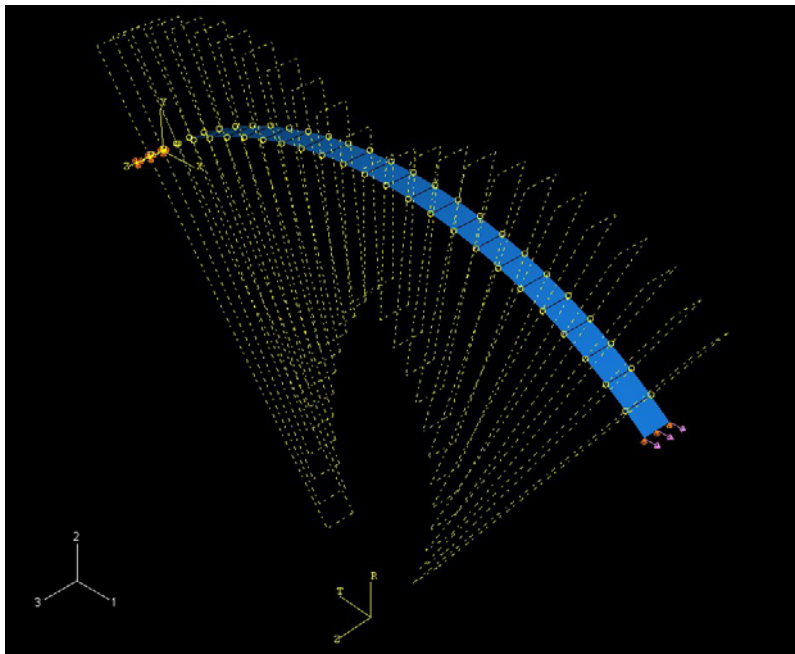


Figure 6. Finite element model

A combination of gravity and transverse load is applied; a boundary condition was applied to the other end such that the translational displacement is zero. Thermal loading is not applied; therefore the flexural curvature depends only on the elastic properties of the material (E_1 , E_2 , ν_{12} , and G_{12}). Eleven loads were applied starting from zero until the value of the maximum load. The value of the curvature was computed for each load. The values of the loads are the same used in experimental tests, thereby establishing a correlation between experimental tests and numerical simulations.

The model has the same dimensions of the strip: length of 260 mm; width of 12 mm. Each ply was measured by means of micrograph and its values were used in the model. The model was divided in 26 parts along the length; therefore each part is 10 mm long by 12 mm wide. Twenty-seven different points were created with a spacing of 10 mm between them. The first point was chosen for the length 0 mm and 260 mm last. The points were chosen with the objective of comparing their positions before and after displacement after the application of load.

The commercial software MSC.NASTRAN® and ABAQUS® do not provide curvature as an output option. However, one can use the displacements of the 27 points previously selected and stored in an output file to compute the curvature change with a MATLAB® subroutine.

A convergence analysis has been carried out to establish the accuracy of the results. Three types of mesh were tested: coarse, medium and very refined. The coarse mesh has 416 ($8 \times 8 \times 26$) elements (remembering that the model was divided into 26 parts). The very refined mesh has 6656 ($16 \times 16 \times 26$) elements and finally an intermediate mesh was used with 1664 ($8 \times 8 \times 26$) elements. The maximum error found between the very refined mesh and the intermediate was less than 0.1%, using the values of curvature as a reference. The maximum computational time spent on non-linear static analysis was less than 5min, quite satisfactory for the computational resource available. In this case, the mesh with 1664 elements was chosen to be used by all models.

According to the ABAQUS documentation, element type S8R5 is most suitable for the model (ABAQUS, 2005). Element type S8R5 is used, since tests have shown this to be the most cost-effective shell element in ABAQUS and provides reasonably accurate results with fine meshes, although the coarse mesh results with these elements demonstrate poor accuracy.

Element type 8R5 is a 8-node doubly curved thin shell, using five degrees of freedom per node. It has three displacement and two rotation variables at an internally generated midbody node. When shell elements with five degrees of freedom per node (S8R5) are used in the global model, the rotations are not written to the results file; therefore, only the displacement degrees of freedom can be driven. The computation uses reduced integration.

For geometrically nonlinear analysis, small-strain shell elements in ABAQUS/Standard (S8R5) use a total Lagrangian strain, and the stress and strain components are given relative to material directions in the reference configuration. For the mechanically loaded case the edge loads are given as point loads on the edge nodes. Since the second-order elements (S8R5) use quadratic interpolation along their edges, consistent distribution of a uniform load gives equivalent point loads in the ratio 1:4:1 at the corner, midside, and corner nodes, respectively (Simpson's integration rule).

This model was used drilling hourglass scaling factor default. Hourglass is energy associated with constraints used to remove singular modes, depend on the shear modulus and are constant for the entire model.

3. RESULTS

The material elastic properties are presented in Tab. 3, Daniel and Ishai (1994). The thermal expansion coefficients were assumed to zero, because the analysis is purely elastic.

Table 3. Elastic properties (Carbon/epoxy AS4/3501-6)

Mechanical property	Value
Longitudinal modulus of elasticity, E_1 (MPa)	142000
Transverse modulus of elasticity, E_2 (MPa)	10300
Shear modulus, G_{12} (MPa)	7200
Major Poisson ratio, ν_{12}	0.27
Thickness, t (mm)	0.18

Daniel and Ishai (2006) suggest using the nominal values of thickness per layer ($t = 0.18$ mm). The average results of 10 micrograph samples are presented in table 1. For $t_{0^\circ} = 180.4 \pm 9.2 \mu\text{m}$ and $t_{90^\circ} = 181.2 \pm 8.4 \mu\text{m}$. Table 2 was presented by the average layer, estimated from measurements of thickness at 54 points along the length. For average layer $t_{0^\circ} = t_{90^\circ} = 0.198 \pm 0.0086 \mu\text{m}$.

Comparison among simulation and experimental results for the cross-ply laminate [0/90] are presented in Fig.7. Three curves were simulated with the goal of correlating its results with the experimental curve. The first curve was simulated with the nominal value suggested by Daniel and Ishai (2006). The second curve was simulated based on the results of the micrographs measurements with standard deviation. The third curve uses the results measured by micrometer with the standard deviation. The graph show a good correlation between the curves generated by ABAQUS and measured by image processing.

4. CONCLUSIONS

The theoretical values compared with the average of the results of micrographs presented a good correlation between them. The correlation of the model with the thickness measurement in Tab. 2 presents the best agreement.

Specialists in manufacturing of composite materials indicate that the lack of uniformity in the laminate can also be obtained from the manufacturing *prepreg* and long period of storage of material still in the form of roll. Thus, one can say that lack homogeneity is due to a number of factors that combined, can increase or decrease the impact of processing on the response of the laminate, and these effects more pronounced rolled into a small thickness.

The curve is strongly influenced by the thickness of the layer. The increase in the value of the thickness of the layer causes an increase in rigidity of the laminate and hence an increase in the value curvature. However, the fibers are in the same direction of the axis of reference (0°) are those that have greater influence on the final value of the curvature, ie a small change in the thickness of the layer to 0° , produces a wide variation in the final value of curvature. A small change in the layer to 90° , has almost negligible influence on the curvature.

5. ACKNOWLEDGEMENTS

The authors wish to thanks Embraer for supplying the material and manufacturing all of the samples used in this work and CAPES by financial support received.

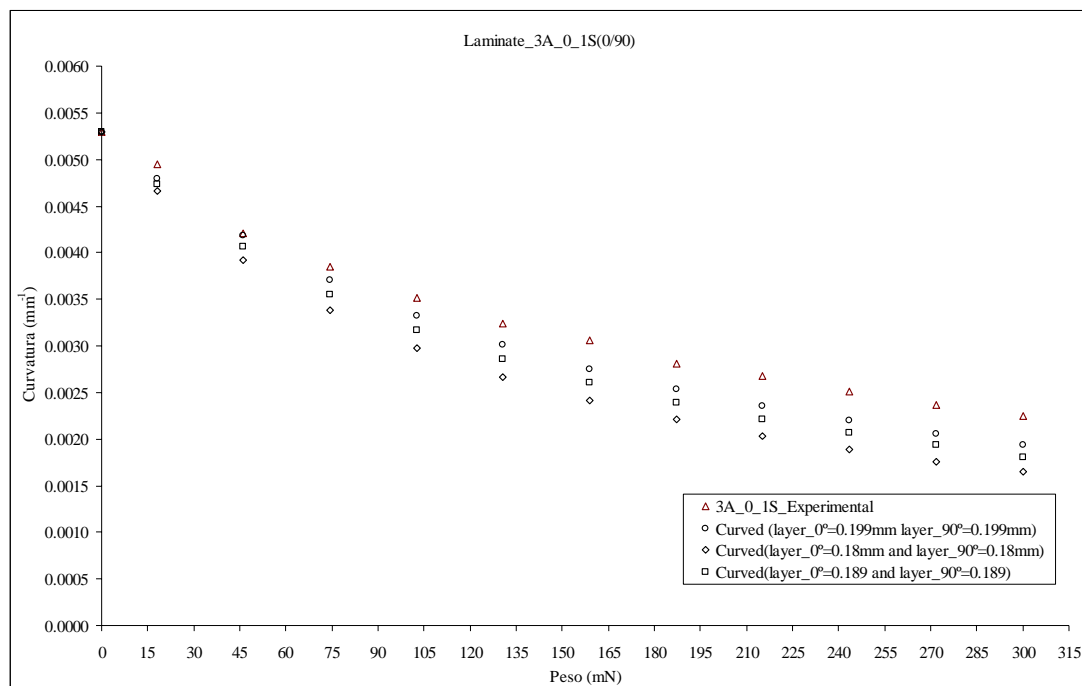


Figure 7. Comparison among simulation and experimental results for the [0/90] laminate

4. REFERENCES

- ASTM D3039/D 3039M-00. Standard test method for tensile properties of polymer matrix composite materials, 2006.
- ABAQUS 6.5-1. Theory manual. 2005.
- BAILLARGEON Y. and VU-KHANH T., 2001 "Prediction of fiber orientation and microstructure of woven fabric composites after forming", Composite Structures, Vol. 52, pp. 475-481.
- DANIEL I. M., ISHAI O., 2006, "Engineering Mechanics of Composite Materials, 2nd edition, Oxford University Press".
- LAROCHE D. and VU-KHANH, T., 1994, "Forming of Woven Fabric Composites", Journal of Composite Materials, Vol. 28, pp. 1825-1839.
- KAM T.Y., CHEN C.M. and YANG S.H. Material characterization of laminated composite materials using a three-point-bending technique. Composite Structures 2009; 88:624-628.
- MSC.NASTRAN® Reference Manual, 2004. MSC Software Corporation.
- OH, S., KIM, K. and KIM, C., 2006, "An efficient postbuckling analysis technique for composite stiffened curved panels", Composite Structures, Vol.74, pp. 361-369.
- PALEROSI, A.C. and ALMEIDA, S.F.M., 2007, "Thermoelastic evaluation of composite laminates using digital imaging processing, Composites Part A: Applied Science and Manufacturing, Vol 38, No. 11, pp.2283-2293.
- PARLEVLJET, P., BERSEE, H.E.N. and BEUKERS, A., 2007, "Residual stresses in thermoplastic composites – a study of the literature. Part III: Effects of thermal residual stresses", Composites: Part A, Vol. 38, pp. 1581-1596.
- The MathWorks, Inc© 1994-2006
- WANG, S.S. and CHOI, I., 1982, "Influence of Fiber Orientation and Ply Thickness on Hygroscopic Boundary-Layer Stresses in Angle-Ply Composite Laminates". Journal of Composite Materials, 16: 244-258.
- RADFORD, D.W., 1993, "Cure shrinkage induced warpage in flat uni-axial composites", Journal of Composite Technology & Research, Vol.15, No. 3, pp290-296.
- RADFORD, D.W. and FU, S.A., 2003, "Route to shape correct/shape stable laminates. In: International Congress of Composite Materials, 14., San Diego, Proceedings... San Diego.

5. RESPOSABILITY NOTICE

The authors are the only responsible for the printed material included in this paper.